Desalination and Water Treatment
www.deswater.com

doi: 10.5004/dwt.2018.22974

130 (2018) 44–53
October

Effects of low-toxicity solvent and binary mixed additives on the microstructure and performance of cellulose triacetate (CTA) membranes for forward osmosis

Chunxia Li[a], Jianfeng Song[b], Pengjia Dou[b], Yong Yin[b], Tao He[b], Weina He[a,*]

[a]*Shanghai Jiao Tong University School of Medicine, Shanghai 200025, China, Tel. +86 21-63846590; Fax: +86 21-63846590 Ext. 776468; emails: wnhe2013@sinano.ac.cn (W. He), lichunxia_8601@hotmail.com (C. Li)*
[b]*Shanghai Advanced Research Institute, Chinese Academy of Sciences, Shanghai 201210, China, Tel. +86 21-20325162; Fax: +86 21-20325034; emails: songjf@sari.ac.cn (J. Song), doupj@shanghaitech.edu.cn (P. Dou), yiny@sari.ac.cn (Y. Yin), het@sari.ac.cn (T. He)*

Received 21 December 2017; Accepted 12 August 2018

ABSTRACT

Cellulose triacetate (CTA) based membranes for forward osmosis (FO) have been prepared with *N*-methyl pyrrolidone (NMP), acetone, and tetrahydrofuran (THF) as solvents and pore forming agents by immersion precipitation. Casting composition and preparation conditions including CTA weight content, NMP/additives ratio, THF/acetone ratio, evaporation time, and coagulation bath temperature (CBT) were systematically investigated for their effects on membrane structure and FO performances. A CTA membrane with the dense skin layer on the surface and sponge-like support layer in the middle was obtained. The CTA membrane showed a water permeability of 10.78 L/(m^2 h) (LMH), higher than 8.70 LMH of commercial Hydration Technologies Inc.(HTI) membrane, and a specific reverse draw solute flux (mass of salt back-diffusion per 1 L pure water produced) of 0.65 g/L, lower than 1.17 g/L of HTI membrane.

Keywords: Low toxicity; Binary mixed additives; Water permeability; Cellulose triacetate; Forward osmosis

1. Introduction

Forward osmosis (FO) is a chemical potential-driven process occurring naturally across the semipermeable membrane. The driving force comes from the water chemical potential gradient between the feed solution (FS) with a high water chemical potential (low osmotic pressure) and the draw solution (DS) with a low water chemical potential (high osmotic pressure). Water diffuses from the feed side to the draw side across the membrane. No hydraulic pressure is applied in the FO process. Further preponderances such as low fouling and better fouling reversibility due to the low compact fouling layer formed have attracted more and more attention. Low energy consumption and low fouling were ever thought as the two remarkable advantage of FO compared with other water treatment technology, such as electric dialysis, reverse osmosis (RO), multistage flash distillation, and so on, when the draw solute was not need to be recycled or recovery cost was relatively low [1]. Its potential applications including water purification [2], wastewater treatment [2–5], saline and seawater desalination [6], pharmaceutical production [7], food processing [8], agriculture and chemical industry [9–11] have been reported. The advantages of FO are manifested in cases where the draw solute is a process components for the industry, thus the recovery is not required [12,13].

The membrane with low internal concentration polarization (ICP), antifouling property, high water permeability, and salt resistance is thought to be the ideal FO membrane. Recently, many research works on the structure and performance promotion of FO membrane have

* Corresponding author.

been published [12,14–18]. Although thin-film composite (TFC) membrane by interfacial polymerization has shown its several advantages, such as high water flux, better salt retention, and wide operating pH [19–22], it has the disadvantage such as weak chlorine tolerance and fouling resistance [23,24]. Cellulose triacetate (CTA) is thought as a suitable polymer for FO membrane due to its easily getting of raw materials, hydrophilicity, and antifouling propensity [25]. The commercial FO membrane belonged to Hydration Technologies Inc. (HTI) is believed to be a CTA-based membrane with a polyester mesh or nonwoven fabrics as the strengthening scaffold [26,27]. In recent years, more research works focused on the development of cellulosic-derived polymer FO membrane generally fabricated by phase inversion. Graphene oxide (GO) was incorporated into CTA membrane to reduce the water resistance and ICP for promoting the hydrophilicity of CTA membrane. The CTA/GO composite membrane showed the water flux high up to 18.43 L/(m^2 h) (LMH) and the specific salt reverse flux low down to 0.22 g/L when deionized (DI) water was FS and 0.5 M NaCl was DS [14]. Meanwhile, the incorporation of GO enhanced the antifouling capability of composite membrane. The CTA membrane with the addition of acetic acid in the solvent system of 1,4-dioxane/acetone exhibited higher water flux of about 20 LMH when 2 M NaCl and DI water were used as DS and FS [23,24]. Based on the 0.5–2.0 M $MgCl_2$ DSs, the CA membrane casted using acetone and formamide as the solvent system exhibits the water flux of 13.57–30.98 LMH with salt leakages in the range of 0.37–1.26 g/m^2/h, respectively [28].

Most cellulosic-derived polymer-based FO membranes were casted by dissolving in 1,4-dioxane solvent system. But it is reported that 1,4-dioxane can cause liver tumors in rodents through cytotoxicity and subsequent regenerative hyperplasia [29] and was classified as "likely to be carcinogenic to humans" by US Environment Protection Agency (USEPA) based on toxicological data [30]. Meanwhile, USEPA recently add 1,4-dioxane on its initial list of 10 "high priority" chemical substances as part of the 2016 amendments to the Toxic Substances Control Act. *N*-Methyl pyrrolidone (NMP) is rather good to dissolve CTA and other polymers [31–33]. Although research works about oral administration of NMP up above 500 mg/kg/d to rats shows toxic effects [34], no one would take NMP by oral administration normally. Another piece of work on NMP metabolites in plasma and urine from volunteers after experimental exposure to NMP in dry and humid air indicated that there was not a statistically higher absorption of NMP after exposure to NMP in humid air than in dry air [35]. NMP shows lower toxicity as compared with 1,4-dioxane.

NMP solvent system was used to dissolve CTA polymer effectively to form homogenous solution in this work. Furthermore, acetone and tetrahydrofuran (THF) were used as binary mixed pore-forming agent and CTA membranes with dense selective layer and sponge-like open-cell network sublayer were successfully prepared. The polymer solution recipe and preparation conditions including CTA content, solvent and additive ratio, evaporation time, and coagulation bath temperature (CBT) were optimized. The optimized membrane performance was compared with the commercial HTI-CTA membrane. The objective of this research work was mainly focused on the establishment of appropriate solvent system for casting CTA FO membrane.

2. Experimental

2.1. Materials

CTA was purchased from Wuxi Institute of Chemical Engineering, with an acetyl content of 43–44 wt.%. Sodium chloride, NMP, acetone, and THF are of analytical grade, obtained from Sinopharm. DI water was used for FO performance test including pure water permeability and salt selectively rejection test. Commercial FO membranes were provided by HTI.

2.2. Membrane preparation

CTA membranes were prepared by immersion precipitation. Firstly, CTA was dried above 40°C at vacuum oven. A weighed amount of dried CTA was added to three-necked flask equipped with a mechanical stirrer containing a premixed solvent of NMP, acetone, and THF at a certain ratio. The solution was kept at 30°C and stirred till a homogeneous solution was obtained, followed by deaeration in an oven at 30°C for several hours before casting. The polymer solution was cast onto a dry and clean glass plate using a casting knife of 150 μm. Then the plate was immersed into a water bath at different temperatures (0°C–40°C) after exposed in the air for a certain time. After solidification and peel off, the membranes were immersed in DI water which was changed every 4 h for 24 h before test. All the membrane prepared under the environment humidity of 50%–55% and temperature of 25°C ± 1°C.

2.3. Scanning electron microscopy

The cross-section morphologies of CTA membranes were characterized using field emission scanning electron microscopy (SEM, Sirion 200). To minimize the morphological change, the freeze-drying technique was utilized. Membrane pieces were fractured in liquid nitrogen and stored in a round bottom flask. The flask with the membrane was connected to the vacuum system in the freeze dryer and immediately kept in liquid nitrogen to maintain a low temperature. After 12 h, the samples were fixed on a specimen stage with the conducting resin and were coated with a thin gold layer for SEM imaging.

2.4. Water uptake test

Porosity of the membranes was estimated gravimetrically using Eq. (1). where ε is the water uptake of the membranes. The membrane with the length of L and the width of b was wiped quickly, and then was weighed as the wet membrane mass w_0. The membrane was set in the air to dry with the dry membrane mass of w_1, ρ_w is water density, and t_0 is the membrane thickness. Water uptake was calculated three times for each sample and the average value was reported.

$$\text{Water uptake} = \frac{\left(w_0 - w_1\right)/\rho_w}{L \times b \times t_0 \times 10^{-4}} \times 100\% \quad (1)$$

2.5. FO performance test

The prepared membranes were tested in a laboratory-scale FO setup, as shown in Fig. 1. The test cell consists of two rectangular plastic symmetric half cells with the membrane in between. The dimensions inside the half cell are 10 cm in length, 3 cm in width, and 0.3 cm in height. 2 L DI water was used as FS and 0.5 M NaCl aqueous solution was used as the DS. Both FS and DSs were circulated using gear pumps. The concurrent FS and DS flow was adopted to reduce the strain on the suspended membrane. The flow rate determined to be 1.8 L/min after optimization test to reduce the external concentration polarization. A circulator maintained both FS and DSs at 25°C ± 0.5°C. Electronic thermometers with accuracy of 0.1°C were used to detect the solution temperature at the inlet and outlet of the module.

FO performance generally was assessed under the FS mode (the FS faced the dense selective layer and the DS faced the support layer) over 1 h, by measuring permeate water flux (J_v) and reverse solute flux (J_s). Calculated data were taken after initial stabilization period of about 10 min. Water flux was calculated by the weight change of the DS due to the water permeation as follows:

$$J_v = \frac{\Delta m}{S_m \times \Delta t \times \rho_w} \tag{2}$$

where J_v is the membrane water flux (kg/m²/h) (in this report same as L/m²/h), Δm is the weight of water passing through the membrane (kg), S_m is membrane area (m²), and Δt is the duration for collecting permeate (h).

In FO processes, reverse solute flux of FO membrane was defined as the amount of NaCl permeating from the DS to the FS per unit membrane area per unit time, showed as J_s, as follows:

$$J_s = \frac{\Delta\left(C_t \times V_t\right)}{S_m \times \Delta t} \tag{3}$$

where C_t and V_t are the salt concentration and the volume of the feed at the end of the FO tests, respectively. The $\Delta(C_t \times V_t)$ is the change of the amount of the salt before and after the test, or the salt diffuse from the DS back to the feed. Duplicated test were carried out in this experiment and average results are reported with standard deviation lower than 10%.

Specific reverse draw solute flux (SRSF) was defined as the amount of NaCl diffused into the FS from DS when producing per liter pure water, showed as J_s/J_v (g/L).

$$\text{SRSF} = \frac{J_s}{J_v} \tag{4}$$

2.6. Membrane structure parameter

In FO process, the solute resistivity K can be determined according to the following equation:

$$K = \left(\frac{1}{J_v}\right)\ln\left(\frac{A\pi_{\text{Draw}} + B}{A\pi_{\text{Feed}} + J_v + B}\right) \tag{5}$$

where π_{Draw} and π_{Feed} represent the osmotic pressure of the FS near the membrane surface and the bulk DS, respectively. A represents the pure water permeability coefficient and B represents the solute permeability coefficient of the

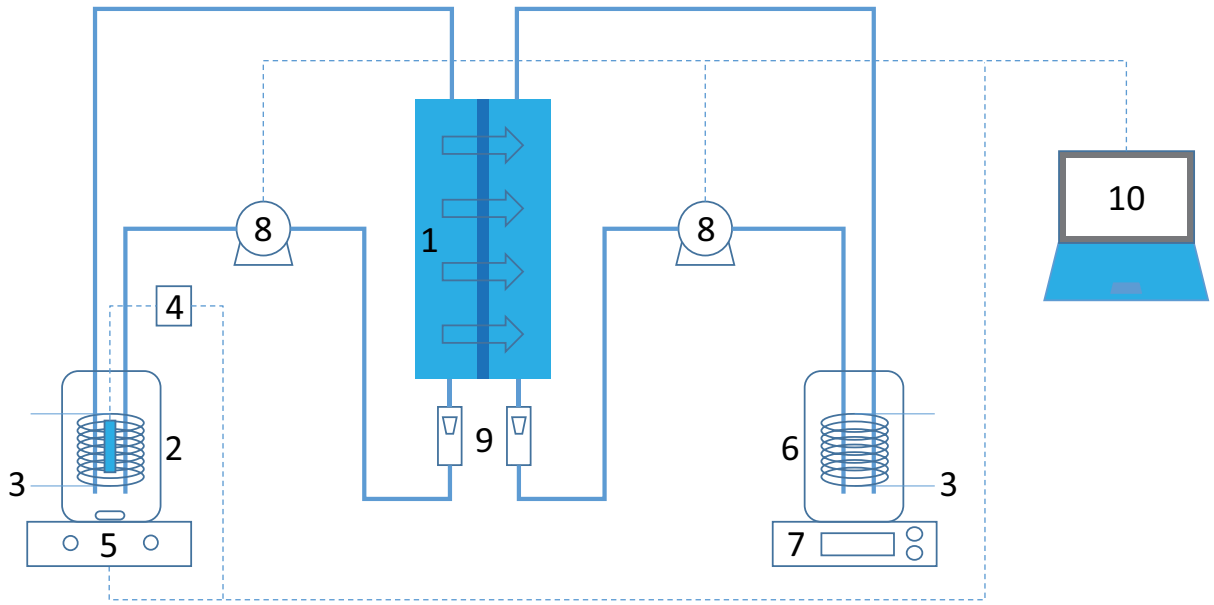

Fig. 1. Schematic diagram of the FO system. (1) membrane module; (2) feed solution container; (3) thermostatic bath; (4) conductivity transmitter; (5) stirrer; (6) draw solution container; (7) digital balance; (8) gear pump; (9) flowmeter; (10) data collection and analysis system. Effective area of the FO membrane cell: 24 cm²; cross-flow velocity of the feed and draw solutions: 25 cm/s; temperature of the feed and draw solutions: 25°C ± 0.5°C.

CTA membrane. They were determined using a RO test setup (Sterlitech Corporation) using the standard protocol described by Cath et al. [36].

The membrane structural parameter (S) is a product of the solute resistivity (K) and the solute diffusivity (D), and is determined by membrane thickness (t_s), membrane tortuosity (τ), and membrane porosity (ε) [36].

$$S = KD = \frac{t_s \tau}{\varepsilon} \tag{6}$$

3. Results and discussion

3.1. Effect of CTA content

Different CTA content membranes with the constant ratio of NMP/additives (1:1.3) and acetone/THF (1:1.5) were prepared and tested. The FO performance characterization of CTA membranes was carried out using DI water as the FS and 0.5 M NaCl aqueous solution as the DS under the mode of active layer facing the FS. Fig. 2 shows the FO performance of membranes prepared by varying the CTA weight fraction from 12 to 16 wt.%.

Water flux J_v decreased from about 10.78 to 7.73 LMH. This is due to higher content of CTA induced higher polymer distribution and then increased the resistance of water molecular permeating the CTA membrane. So, water flux decreased with increasing CTA content in the casting membrane solution. The specific reverse solute flux (J_s/J_v) is the ratio of reverse solute loss per unit permeate water, reflects the membrane selectivity. The less SRSF value indicates higher reject rate and better selectivity. The SRSF is thought to be closely related with the dense layer of membranes. More compact is the dense layer, the SRSF value is less, which accounts for that better salt rejection rate may work in the application. As seen in Fig. 2, the SRSF varied slightly when the CTA weight fraction was between 12 and 15 wt.%. But when CTA content reached at 16 wt.%, the SRSF decreased sharply from about 0.65 to 0.50 g/L. That is to say the selectivity of the CTA membrane was promoted by a large margin as the polymer content increased to 16 wt.%. This may be explained by that enough polymer chain can be conjunct with others to form enough dense layer with high selectivity and then salt molecular permeating across the membrane per unit hour showed a sharply decrease when the CTA content is increased enough to 16 wt.%.

3.2. Effect of NMP/additives

CTA is hard to be dissolved because its high acetyl content about 43–44 wt.%. NMP is a better solvent for CTA and is more friendly to research worker and environment compared with dioxane with stronger toxicity and carcinogenicity [29], which is usually used for CTA solvent. In this section, by fixing CTA content at 12 wt.%, THF/acetone at 1:1.5 and varying the NMP/additives from 1:2.3 to 1:0.8, different CTA membranes were prepared. FO performance of these membranes was characterized in FS mode.

The effects of NMP ratio in the casting solution were investigated on water permeability and SRSF as shown in Fig. 3. The water permeability increased obviously from about 8.0 to 15 LMH when the NMP/additives ratio varied from 1:2.3 to 1:0.8. NMP has the biggest dispersive and dipole–dipole solubility parameter, as seen in Table 1, so NMP was the best solvent for CTA among the system.

The compatibility between the ring system of NMP and the pyranose ring of CTA molecular is the reason for it [37]. Stronger interaction between the solvent and polymer can form when higher content of NMP is used in the casting solution. When a pristine membrane is immersed into the coagulation bath, the nonsolvent will diffuse into the polymer matrix and the solvent in the matrix will diffuse out to the coagulation bath because of the chemical potential difference. Stronger interaction between the solvent and polymer decelerates outflow of the solvent, and so indirectly promotes the inflow of nonsolvent to the matrix. In this case, the casting solution can reach liquid–liquid phase separation at lower polymer concentration [37] and the corresponding membrane porosity is higher. In other words, the membrane prepared using higher content of NMP will show higher water flux in the FO test. This is the reason that

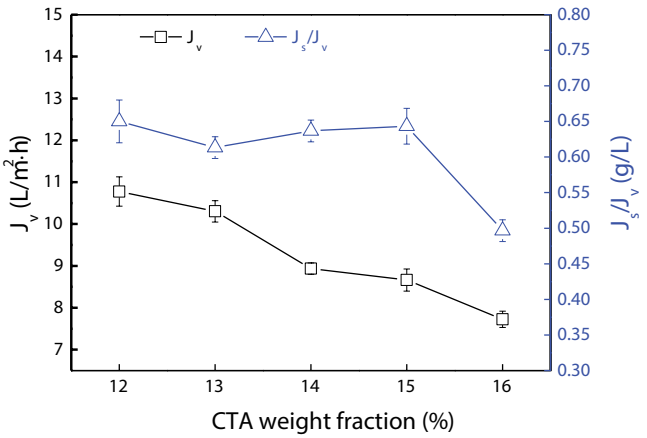

Fig. 2. Effect of CTA weight fraction on J_v and J_s/J_v. NMP/additives = 1:1.3; THF/acetone = 1:1.5; CBT 27°C; evaporation time 20 s.

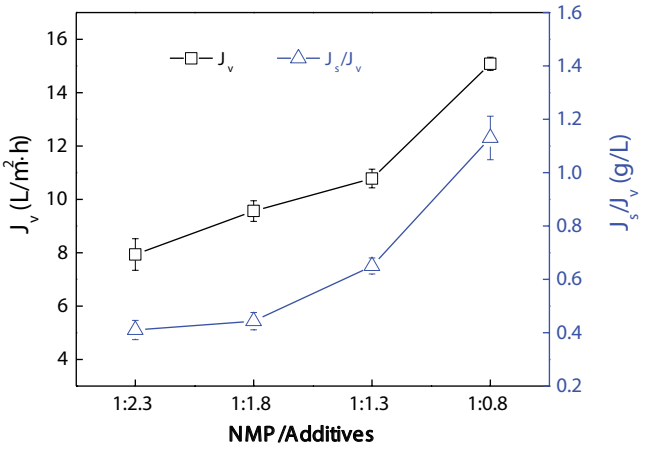

Fig. 3. Effect of NMP/additives on the forward performance of membrane. THF/acetone = 1:1.5; CTA content 12 wt.%; CBT 27°C; evaporation time 20 s.

Table 1
Solubility parameter of liquids at 25°C and polymer [38]

Compounds	δ_d (MPa)$^{1/2}$	δ_p (MPa)$^{1/2}$	δ_h (MPa)$^{1/2}$	Solubility parameter (MPa)$^{1/2}$ δ
THF	16.8	5.7	8.0	19.4
Acetone [37]	15.5	10.4	7.0	20.1
NMP	18.0	12.3	7.2	23
CTA [37]	15.6	–	10.4	18.8

the water permeability is increasing with the arising NMP content.

The SRSF shows increasing trend with the augment of *NMP* content in the system as seen in Fig. 3. The J_s/J_v exhibits the least value of 0.41 g/L when the ratio of NMP/additives was fixed at 1:2.3 but the water flux is only 7.93 LMH. Water permeability and SRSF increased when more NMP was used in the casting solution. This can be explained by that good solvent for polymer can induce the liquid–liquid phase separation at lower polymer concentration in the matrix [37,39]. Accordingly, the polymer content in the dense layer is also lower and the compactness of selective layer is worse. So, salt flux and J_s/J_v both increased. Another reason for the increasing of SRSF with *NMP* content is that acetone and THF have greater saturated vapor pressure of 49.14 and 15.20 kPa than NMP of less than 0.133 kPa at 15°C [40]. Decreasing acetone and THF content results in less solvent evaporation and hence a lower polymer concentration on the membrane surface. Consequently, a less dense skin layer was formed, leading to a higher SRSF.

3.3. Effect of THF/ACT

The membrane casting solution contains two high volatile components: acetone and THF, which affects the pore structure and FO performance seriously. Fig. 4 shows FO performance of membrane casted using different ratio of THF and acetone. The water flux and SRSF both display rising trend with the decreasing THF ratio. That means that

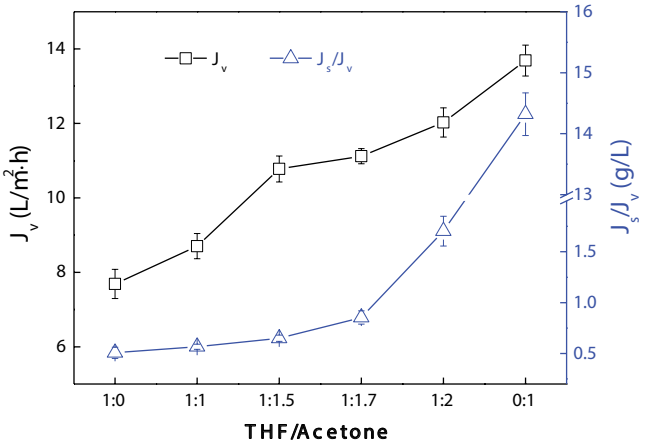

Fig. 4. Effect of THF/acetone on the forward performance of membrane. S/NS = 1:1.3; CTA content 12 wt.%; CBT 27°C; evaporation time 20 s.

THF is beneficial to improve the compactness of skin layer and salt rejection capacity of membrane.

Generally, membranes with a more porous top layer would be obtained due to instantaneous liquid–liquid demixing, whereas membranes with a dense skin layer would be obtained following delayed demixing [39]. Formation of a dense skin layer requires a high polymer content before liquid–liquid phase separation. THF has the lowest mutual affinity with water as compared with acetone and NMP (Table 1), both have the carbonyl in the molecule. Consequently, addition of THF into the solution contributes to the delayed demixing [41].

The compactness of the skin layer and the pore connectivity are decided by the polymer-rich phase and polymer-poor phase. On one hand, high THF ratio allows more solvent (such as NMP and acetone) to diffuse out of the polymer solution. On the other hand, there is more time for CTA polymer molecular chain entanglement and for the polymer-rich phase to grow up at high THF ratio because of promoted delayed liquid–liquid demixing. Based on above reasons, more compact skin layer was formed at high THF ratio leading to lower J_s/J_v value. The cross-section photographs of membranes with different ratios of THF and acetone are shown in Fig. 5. The CTA membranes with skin layer of a certain depth have been obtained in accordance with the PAS characterization of CTA membrane by Ong and Chung [42]. The pore connectivity would be sacrificed as shown in Figs. 5(c1) and (c2) corresponding to the high THF ratio. The connectivity is promoted when acetone ratio is increased as shown in Figs. 5(c3) and (c4). The morphologies in Figs. 5(a4), (b4), and (c4) show the CTA membrane has a fully porous open-cell network structure in the sublayer and a relatively dense skin layer, which can support the research works of Ong and Chung [42]. The water permeability increased as the THF content is reduced due to the improved pore connectivity. At reduced THF content, weakened instantaneous liquid–liquid demixing leads to less compact skin, SRSF increased following a decrease of THF content.

3.4. Effect of evaporation time

The pristine membranes were set in the environmental temperature and humidity of about 25°C and 50%–55%, respectively, for varied evaporation time from 3 to 60 s before they were immersed into the coagulation bath. Fig. 6 shows the effect of the evaporation time on the water flux and SRSF. The water permeability increased from 9.33 to 13.54 LMH as the evaporation time extended, due to the increase in the membrane porosity as shown in Appendix. The J_s/J_v increased from 0.60 to 0.76 g/L as the evaporation

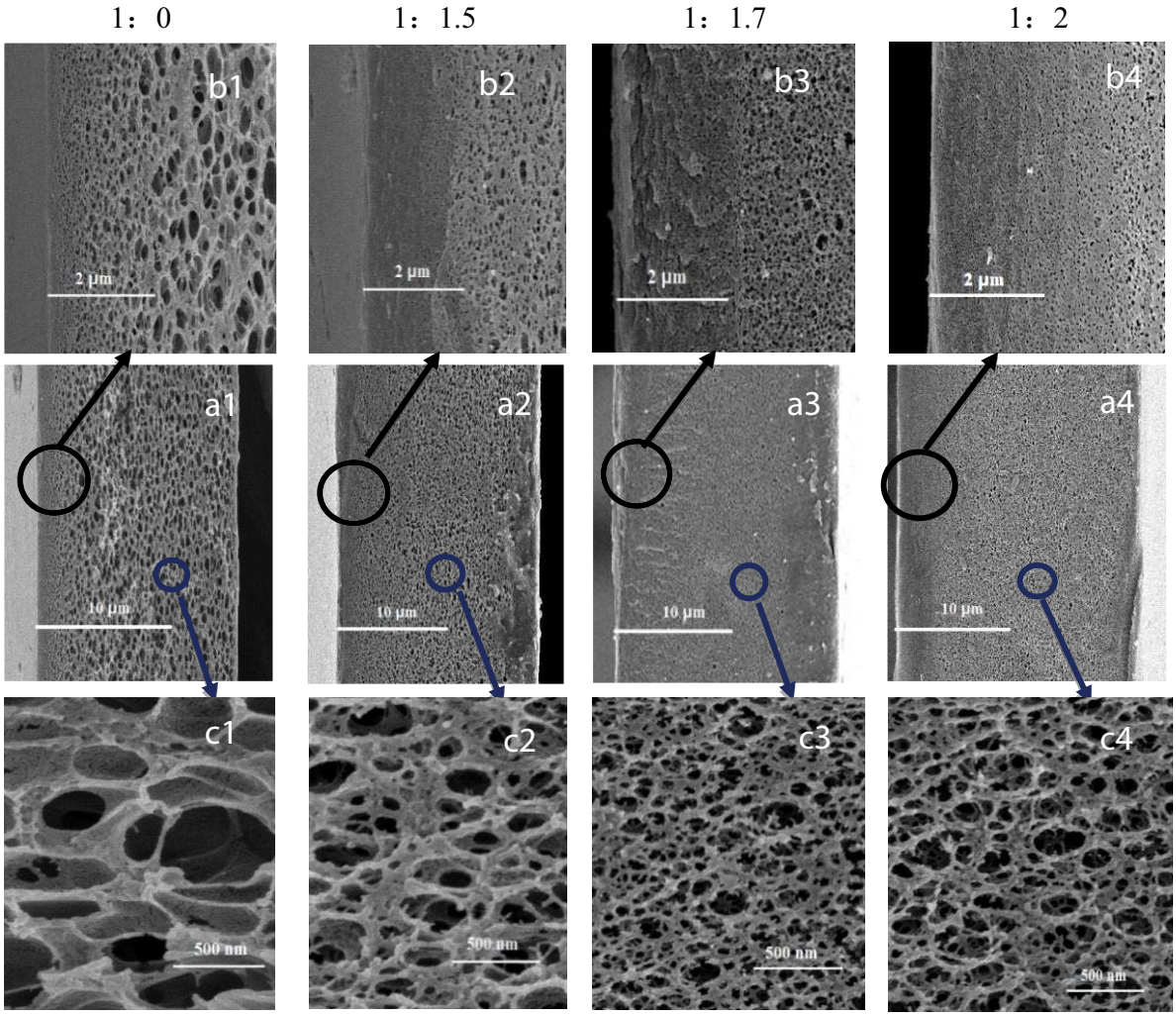

Fig. 5. Morphology of CTA membranes prepared with different ratio of THF and acetone of 1:0, 1:1.5, 1:1.7, and 1:2. (a1–a4) cross-section; (b1–b4) magnification of skin layer edge marked with black circle on (a); (c1–c4) magnification of sublayer marked with blue circle on (a).

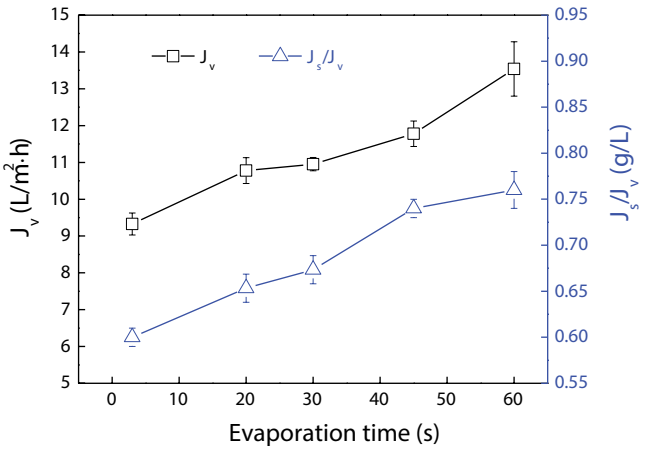

Fig. 6. Effect of evaporation time on the forward performance of membrane. S/NS = 1:1.3; CTA content 12 wt.%; THF/acetone = 1:1.5; CBT 27°C.

time increased from 3 to 60 s. The effect of evaporation time on membrane characteristics can be analyzed from two respects: (1) to increase the number of aggregation pores on the membrane surface and (2) excessive evaporation results in aggregation pores reunion, hence the numbers of pores decreases and the pore size increases [43], as shown in the cross-section (Fig. 7).

The dense layer of 20 s is deeper than that of 30 s from the morphology as shown in Figs. 7(b1) and (b2). This means that the rejection of membrane deteriorated as evaporation time was extended, resulting in increased SRSF. The pore size and porosity both increased obviously with evaporation time as seen in Figs. 7(c1) and (c2), in accordance with the porosity characterization result as shown in Appendix. This also explains the enhanced permeability as the evaporation time is extended. The highly evaporative character of THF than both acetone and NMP will lead to less THF left in the pristine membrane as the evaporation time is extended. Similar to the results in Section 3.3, less THF would lead to higher water flux and lower rejection.

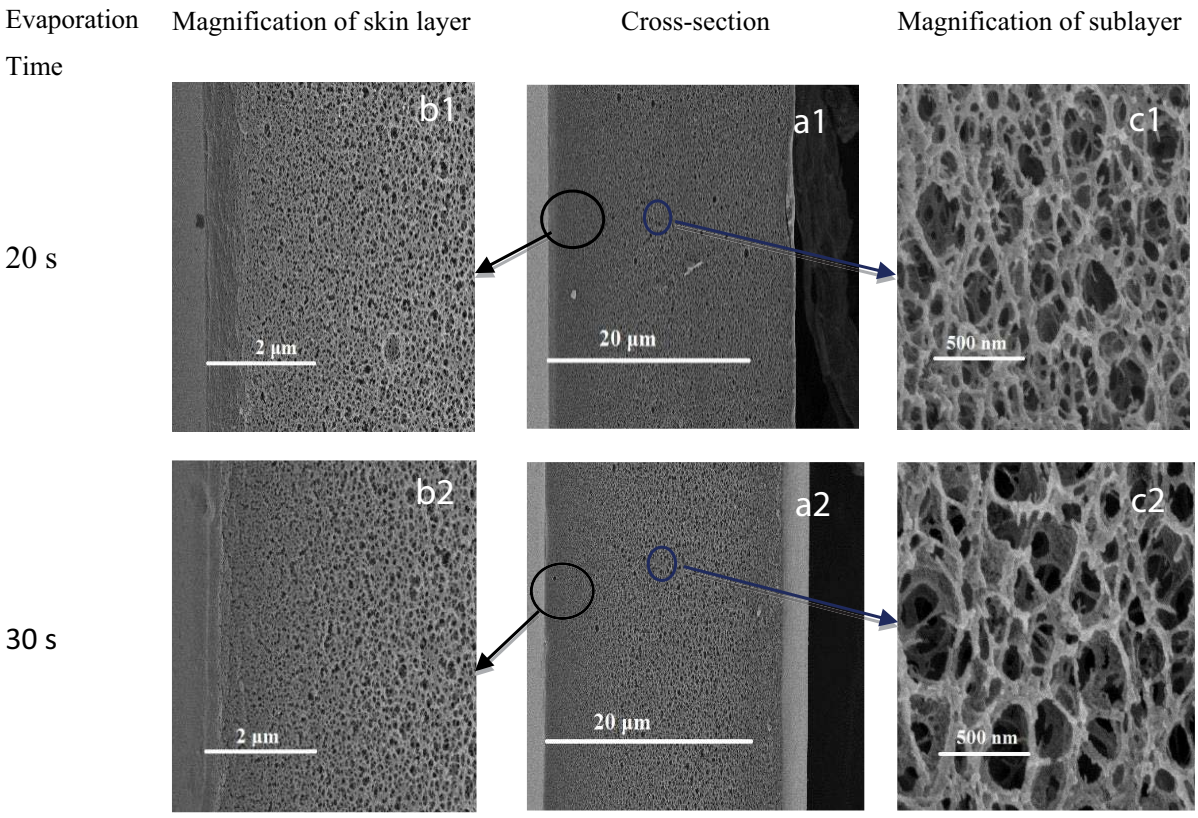

Fig. 7. Morphology of CTA membranes prepared via different evaporation time of 20 and 30 s. S/NS = 1:1.3; THF/acetone = 1:1.5; CTA content 12 wt.%; CBT 27°C.

3.5. Effect of coagulation bath temperature

FO performances of CTA membranes prepared at different CBT were investigated. The results are illustrated in Fig. 8. As the CBT increased from 3°C to 27°C, water flux J_v increased from 6.69 to 10.78 LMH. The J_s/J_v decreased from 1.48 to 0.56 g/L when the CBT varied from 3°C to 37°C. This indicates the compactness of skin layer is enhanced in the high temperature water bath. Fundamentally, this is because relatively higher temperature would cause a shrinkage of voids between nodule aggregates [28]. It is speculated that low temperature is not benefit for CTA molecular chain conjunction because the supplied energy for molecular motion is too low. So, there were much large spaces between intramolecular CTA chain and large voids between polymer aggregates in the membrane [44]. These large voids supplied channels for salts easily passing through the membrane from draw side into feed side. Consequently, the effect of osmotic pressure difference, which is the driving force of water migration from the feed to the DS, was decreased, resulting in the low water permeability [42]. At higher CBT, polymer molecular chains more easily connect by hydrogen bond and coalescence of polymer aggregates takes place. The voids between polymer aggregates shrink and the compactness of skin layer is enhanced [45]. Resistance of salts passing through the membrane and effect of osmotic pressure difference are both increased. Due to the above analysis, the salt leakage decreased and water permeability increased with increasing CBT can be explained.

However, water flux J_v decreased to 9.24 LMH when the CBT was elevated to 37°C. The SRSF of 0.56 g/L is rather low as the coagulation bath is 37°C, which states much few salt leakage happened. In other words, the compactness of skin layer is further promoted due to the further shrinkage of the voids between polymer aggregates, which can be supported by the research of Su et al. [28,45]. A higher temperature benefits the rearrangement of the CTA chains at the skin layer before the CTA chains are completely fixed by gelation [46]. So the salts migrated into the membrane but they mostly could not pass through the skin layer resulting in more severe ICP. This is the reason for the decline of water permeability.

3.6. Performance of CTA membranes in the FO

The optimized polymer solution composition was fixed at 12 wt.% CTA, the weight ratio of NMP and additives at 1:1.3, the weight ratio of THF and acetone at 1:1.5. The solution was casted onto a glass plate followed by the evaporation for 20 s and then immersed into the coagulation bath at 27°C. The CTA membranes prepared under above conditions were tested in the FO process in FS mode when 0.5, 1.0, 1.5, and 2.0 M NaCl solution were used as the DS and DI water as the FS. The water flux and SRSF, as listed in Table 2, both increased with increasing DS concentration. The reason is that the net driving force across the membrane is enhanced for both water and NaCl at high concentration of DS.

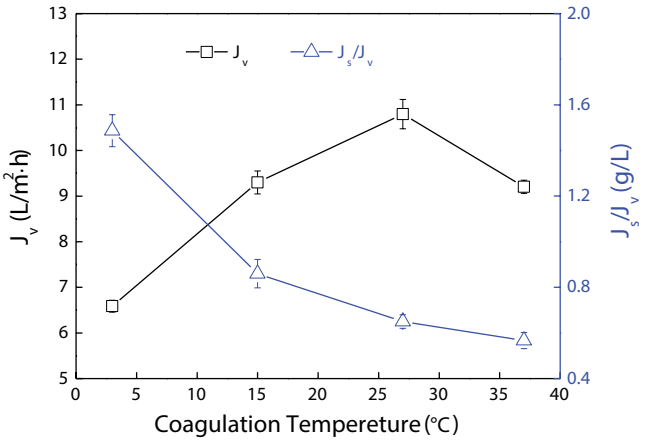

Fig. 8. Effect of CBT on the forward performance of membrane, J_v and J_s/J_v. S/NS = 1:1.3; CTA content 12 wt.%; THF/Acetone = 1:1.5, evaporation time 20 s.

Table 2
Performance of laboratory-made CTA membrane in the FO process

Results	Draw solution concentration (M)			
	0.5	1.0	1.5	2.0
J_v (LMH)	10.78 ± 0.32	16.10 ± 0.25	21.38 ± 0.63	24.35 ± 0.46
J_s/J_v (g/L)	0.65 ± 0.03	0.91 ± 0.02	1.28 ± 0.08	1.41 ± 0.14

Table 3
FO performance comparison between commercial and laboratory-made CTA membranes

Membrane	J_v (LMH)	J_s/J_v (g/L)	DS/FS
HTI-CTA [37]	~5.25	~3.01	1 M KBr/0.1 M NaCl
HTI-CTA [14]	~6.10	–	0.5 M NaCl/DI water
HTI-CTA[a]	8.70	1.17	0.5 M NaCl/DI water
HTI-CTA [46]	~3.7	–	2 M glucose/0.5 M NaCl
Laboratory-made CTA[a]	10.78	0.65	0.5M NaCl/DI water

[a]FO performance of the membrane is tested at the laboratory.

The performance of the optimized laboratory-made CTA membrane was compared against commercial CTA membranes under FS mode as listed in Table 3. The water flux of laboratory-made CTA membrane was about 24% higher than the highest value of selected HTI-CTA membrane. Meanwhile, the SRSF J_s/J_v of laboratory-made CTA membrane was about 45% lower than that of HTI-CTA. Current tailor-made CTA membranes showed better performance than the commercial CTA membranes.

The membrane structure parameters of between laboratory-made CTA membrane and commercial HTI-CTA membrane are shown in Table 4. The A value of the CTA membrane was 0.67 L/m² h bar, slightly lower than that of commercial membrane, 0.79 L/m² h bar, but the structure parameter of the tailor-made CTA membrane was 372 mm, below that of HTI CTA membrane (421 mm). The low S value of current CTA membrane indicates that the ICP of the laboratory-made CTA membrane is less than commercial membrane. Further improvement in the performance of CTA FO membrane could be followed by addition of nanoparticles and other additives into the dope solution to increase the pore connectivity. We will report out further results in the next paper.

Table 4
Structure parameters of prepared CTA membranes.

Membrane	Water permeability A (L/m²/h/bar)	B value (10^{-7} m/s)	S value (mm)
Laboratory-made CTA	0.67	2.74	372
HTI-CTA	0.79	2.39	421

FO test conditions: 0.5 M NaCl as the draw solution and DI water as the feed.

4. Conclusions

An asymmetric CTA membrane for FO process was prepared and systematic investigation was carried out on the preparation conditions, membrane morphology, water uptake, pure water permeability, and SRSF. It was found that water flux and SRSF decreased with increasing CTA content, while they increased with ascending of NMP/additives ratio and THF/acetone ratio. The results indicated that THF and acetone played important roles in affecting the membrane structure and FO performances. Acetone benefited the water flux but reduced the salt resistance. When the ratio of THF/acetone was increased over 1:1.7, pure water permeability and SRSF would increase more rapidly due to the macropore seen in SEM morphology of membrane cross-section and more defect in the skin layer. Prolonged evaporation time led to higher water flux but low salt resistance due to the loss of volatile pore forming agents. Higher temperature of coagulation bath led to less SRSF. While bath temperature induced different effects on the pure water permeability because release of solvent and additives from the polymer matrix and rearrangement of polymer chain happened in different extent when the CBT was below or above 27°C. The laboratory-made CTA membrane showed higher water permeability and better salt resistance than the commercial HTI-CTA membrane.

Acknowledgment

The authors would like to thank the partial financial support from the National Natural Science Fund China (U1507117, 21676290), Shanghai Municipal Commission of Health and Family Planning (20154Y0025), Shanghai Jiao Tong University Medical-Engineering Cross Fund (YG2015QN49), and Shanghai Education Committee (ZZjdyx15014).

References

[1] Q. She, R. Wang, A.G. Fane, C.Y. Tang, Membrane fouling in osmotically driven membrane processes: a review, J. Membr. Sci., 499 (2016) 201–233.

[2] S. Jamil, S. Jeong, S. Vigneswaran, Application of pressure assisted forward osmosis for water purification and reuse of reverse osmosis concentrate from a water reclamation plant, Sep. Purif. Technol., 171 (2016) 182–190.
[3] S. You, J. Lu, C.Y. Tang, X. Wang, Rejection of heavy metals in acidic wastewater by a novel thin-film inorganic forward osmosis membrane, Chem. Eng. J., 320 (2017) 532–538.
[4] S. Lee, Y.C. Kim, Calcium carbonate scaling by reverse draw solute diffusion in a forward osmosis membrane for shale gas wastewater treatment, J. Membr. Sci., 522 (2017) 257–266.
[5] K. Lutchmiah, A.R.D. Verliefde, K. Roest, L.C. Rietveld, E.R. Cornelissen, Forward osmosis for application in wastewater treatment: a review, Water Res., 58 (2014) 179–197.
[6] D. Roy, M. Rahni, P. Pierre, V. Yargeau, Forward osmosis for the concentration and reuse of process saline wastewater, Chem. Eng. J., 287 (2016) 277–284.
[7] Y.-N. Wang, R. Wang, W. Li, C.Y. Tang, Whey recovery using forward osmosis – evaluating the factors limiting the flux performance, J. Membr. Sci., 533 (2017) 179–189.
[8] K.B. Petrotos, A.V. Tsiadi, E. Poirazis, D. Papadopoulos, H. Petropakis, P. Gkoutsidis, A description of a flat geometry direct osmotic concentrator to concentrate tomato juice at ambient temperature and low pressure, J. Food Eng., 97 (2010) 235–242.
[9] M. Shibuya, K. Sasaki, Y. Tanaka, M. Yasukawa, T. Takahashi, A. Kondo, H. Matsuyama, Development of combined nanofiltration and forward osmosis process for production of ethanol from pretreated rice straw, Bioresour. Technol., 235 (2017) 405–410.
[10] L. Chekli, J.E. Kim, I. El Saliby, Y. Kim, S. Phuntsho, S. Li, N. Ghaffour, T. Leiknes, H. Kyong Shon, Fertilizer drawn forward osmosis process for sustainable water reuse to grow hydroponic lettuce using commercial nutrient solution, Sep. Purif. Technol., 181 (2017) 18–28.
[11] L. Chekli, Y. Kim, S. Phuntsho, S. Li, N. Ghaffour, T. Leiknes, H.K. Shon, Evaluation of fertilizer-drawn forward osmosis for sustainable agriculture and water reuse in arid regions, J. Environ. Manage., 187 (2017) 137–145.
[12] X. Li, T. He, P. Dou, S. Zhao, 2.5 Forward Osmosis and Forward Osmosis Membranes, E. Drioli, L. Giorno, E. Fontananova, Eds., Comprehensive Membrane Science and Engineering, 2nd ed., Elsevier, Oxford, 2017, pp. 95–123.
[13] Y. Hartanto, M. Zargar, X. Cui, Y. Shen, B. Jin, S. Dai, Thermoresponsive cationic copolymer microgels as high performance draw agents in forward osmosis desalination, J. Membr. Sci., 518 (2016) 273–281.
[14] X. Wang, X. Wang, P. Xiao, J. Li, E. Tian, Y. Zhao, Y. Ren, High water permeable free-standing cellulose triacetate/graphene oxide membrane with enhanced antibiofouling and mechanical properties for forward osmosis, Colloids Surf., A, 508 (2016) 327–335.
[15] S. Lim, M.J. Park, S. Phuntsho, L.D. Tijing, G.M. Nisola, W.-G. Shim, W.-J. Chung, H.K. Shon, Dual-layered nano-composite substrate membrane based on polysulfone/graphene oxide for mitigating internal concentration polarization in forward osmosis, Polymer, 110 (2017) 36–48.
[16] H. Salehi, M. Rastgar, A. Shakeri, Anti-fouling and high water permeable forward osmosis membrane fabricated via layer by layer assembly of chitosan/graphene oxide, Appl. Surf. Sci., 413 (2017) 99–108.
[17] L. Shen, J. Zuo, Y. Wang, Tris(2-aminoethyl)amine in-situ modified thin-film composite membranes for forward osmosis applications, J. Membr. Sci., 537 (2017) 186–201.
[18] S. Zhang, P. Liu, Y. Chen, J. Jin, L. Hu, X. Jian, Preparation of thermally stable composite forward osmosis hollow fiber membranes based on copoly(phthalazinone biphenyl ether sulfone) substrates, Chem. Eng. Sci., 166 (2017) 91–100.
[19] N.L. Le, N.M.S. Bettahalli, S.P. Nunes, T.-S. Chung, Outer-selective thin film composite (TFC) hollow fiber membranes for osmotic power generation, J. Membr. Sci., 505 (2016) 157–166.
[20] J. Wei, X. Liu, C. Qiu, R. Wang, C.Y. Tang, Influence of monomer concentrations on the performance of polyamide-based thin film composite forward osmosis membranes, J. Membr. Sci., 381 (2011) 110–117.
[21] A.F. Faria, C. Liu, M. Xie, F. Perreault, L.D. Nghiem, J. Ma, M. Elimelech, Thin-film composite forward osmosis membranes functionalized with graphene oxide–silver nanocomposites for biofouling control, J. Membr. Sci., 525 (2017) 146–156.
[22] P. Xiao, L.D. Nghiem, Y. Yin, X.-M. Li, M. Zhang, G. Chen, J. Song, T. He, A sacrificial-layer approach to fabricate polysulfone support for forward osmosis thin-film composite membranes with reduced internal concentration polarisation, J. Membr. Sci., 481 (2015) 106–114.
[23] D. Li, Y. Yan, H. Wang, Recent advances in polymer and polymer composite membranes for reverse and forward osmosis processes, Prog. Polym. Sci., 61 (2016) 104–155.
[24] E. Yang, C.-M. Kim, J.-h. Song, H. Ki, M.-H. Ham, I.S. Kim, Enhanced desalination performance of forward osmosis membranes based on reduced graphene oxide laminates coated with hydrophilic polydopamine, Carbon, 117 (2017) 293–300.
[25] N.M. Mazlan, P. Marchetti, H.A. Maples, B. Gu, S. Karan, A. Bismarck, A.G. Livingston, Organic fouling behaviour of structurally and chemically different forward osmosis membranes – a study of cellulose triacetate and thin film composite membranes, J. Membr. Sci., 520 (2016) 247–261.
[26] T.-S. Chung, S. Zhang, K.Y. Wang, J. Su, M.M. Ling, Forward osmosis processes: yesterday, today and tomorrow, Desalination, 287 (2012) 78–81.
[27] T. Cath, A. Childress, M. Elimelech, Forward osmosis: principles, applications, and recent developments, J. Membr. Sci., 281 (2006) 70–87.
[28] J. Su, S. Zhang, H. Chen, H. Chen, Y.C. Jean, T.-S. Chung, Effects of annealing on the microstructure and performance of cellulose acetate membranes for pressure-retarded osmosis processes, J. Membr. Sci., 364 (2010) 344–353.
[29] M.L. Dourson, J. Higginbotham, J. Crum, H. Burleigh-Flayer, P. Nance, N.D. Forsberg, M. Lafranconi, J. Reichard, Update: Mode of action (MOA) for liver tumors induced by oral exposure to 1,4-dioxane, Regul. Toxicol. Pharmacol., 88 (2017) 45–55.
[30] D.T. Adamson, E.A. Pina, A.E. Cartwright, S.R. Rauch, R. Hunter Anderson, T. Mohr, J.A. Connor, 1,4-Dioxane drinking water occurrence data from the third unregulated contaminant monitoring rule, Sci. Total Environ., 596–597 (2017) 236–245.
[31] S. Zhang, K.Y. Wang, T.-S. Chung, H. Chen, Y.C. Jean, G. Amy, Well-constructed cellulose acetate membranes for forward osmosis: minimized internal concentration polarization with an ultra-thin selective layer, J. Membr. Sci., 360 (2010) 522–535.
[32] A. Figoli, T. Marino, S. Simone, E. Di Nicolò, X.M. Li, T. He, S. Tornaghi, E. Drioli, Towards non-toxic solvents for membrane preparation: a review, Green Chem., 16 (2014) 4034.
[33] Z. Li, J. Ren, A.G. Fane, D.F. Li, F.-S. Wong, Influence of solvent on the structure and performance of cellulose acetate membranes, J. Membr. Sci., 279 (2006) 601–607.
[34] A.M. Saillenfait, F. Gallissot, I. Langonné, J.P. Sabaté, Developmental toxicity of N-methyl-2-pyrrolidone administered orally to rats, Food Chem. Toxicol., 40 (2002) 1705–1712.
[35] M.A. Carnerup, M. Spanne, B.A. Jonsson, Levels of N-methyl-2-pyrrolidone (NMP) and its metabolites in plasma and urine from volunteers after experimental exposure to NMP in dry and humid air, Toxicol. Lett., 162 (2006) 139–145.
[36] T.Y. Cath, M. Elimelech, J.R. McCutcheon, R.L. McGinnis, A. Achilli, D. Anastasio, A.R. Brady, A.E. Childress, I.V. Farr, N.T. Hancock, J. Lampi, L.D. Nghiem, M. Xie, N.Y. Yip, Standard methodology for evaluating membrane performance in osmotically driven membrane processes, Desalination, 312 (2013) 31–38.
[37] T.P.N. Nguyen, E.-T. Yun, I.-C. Kim, Y.-N. Kwon, Preparation of cellulose triacetate/cellulose acetate (CTA/CA)-based membranes for forward osmosis, J. Membr. Sci., 433 (2013) 49–59.
[38] C.M. Hansen, Hansen Solubility Parameters A User's Handbook, CRC Press, New York, 2006.

[39] M. Mulder, Basic Principles of Membrane Technology, Kluwer Academic Publishers, Dordrecht, 1996.
[40] J.G. Speight, Lange's Handbook of Chemistry, McGraw-Hill Companies, Inc., Wyoming, 1972.
[41] M. Mulder, Basic Principles of Membrane Technology, Kluwer Academic Publishers, London, 1997.
[42] R.C. Ong, T.-S. Chung, Fabrication and positron annihilation spectroscopy (PAS) characterization of cellulose triacetate membranes for forward osmosis, J. Membr. Sci., 394–395 (2012) 230–240.
[43] T.A. Tweddle, W.S. Peterson, A.E. Fouda, S. Sourirajan, Effect of casting variables on the performance of tubular cellulose acetate reverse osmosis membranes, Ind. Eng. Chem. Prod. Res. Dev., 20 (1981) 496–501.
[44] R.E. Kesting, Four tiers of structure integrally skinned phase inversion membranes and their relevance to the various separation regimes, J. Appl. Polym. Sci., 41 (1990) 2739–2752.
[45] J. Su, Q. Yang, J.F. Teo, T.-S. Chung, Cellulose acetate nanofiltration hollow fiber membranes for forward osmosis processes, J. Membr. Sci., 355 (2010) 36–44.
[46] G. Li, X.-M. Li, T. He, B. Jiang, C. Gao, Cellulose triacetate forward osmosis membranes: preparation and characterization, Desal. Wat. Treat., 51 (2013) 2656–2665.

Appendix

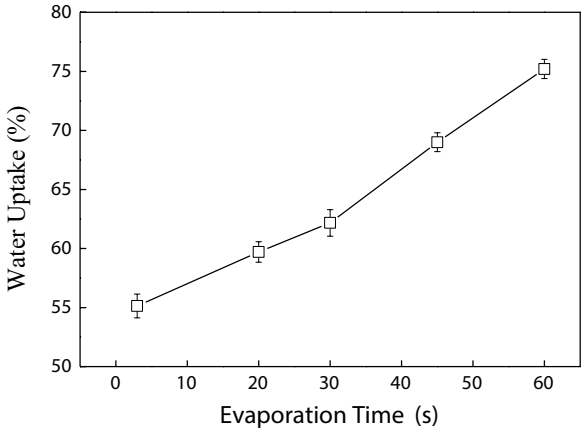

Effect of evaporation time on the membrane water uptake. S/NS = 1:1.3; THF/acetone = 1:1.5; CTA content 12 wt.%; CBT 27°C.